Experimental Range Extension of Concurrent Cooperative Transmission in Indoor Environments at 2.4GHz

Haejoon Jung, Yong Jun Chang, and Mary Ann Ingram
School of Electrical and Computer Engineering
Georgia Institute of Technology
Email: {hjung35, yongjun.chang, mai}@gatech.edu

***Abstract*—Concurrent cooperative transmission (CCT) is a cooperative transmission (CT) technique where multiple radios transmit diversity versions of the same message at the same time. Through array gain and diversity gain, CCT achieves a signal-to-noise (SNR) advantage, which can be used for better link reliability and transmission range extension. CCT range extension can enable broadcasting with fewer hops, balance energy in wireless sensor networks, and overcome network partitions. However, there are few experimental studies of CT range extension in the literature. In this paper, we consider two-hop directional range extension and two-hop coverage area extension as function of relay cluster topology. In particular, we measure average packet error rate (APER), which is averaged over multipath fading. We estimate path loss and shadowing parameters from the APER, and compare outage rate contours based on the log-distance path loss model to the measured APERs.**

I. Introduction

Cooperative transmission (CT) in wireless communication is a way of achieving an SNR advantage in a receiver by combining the transmissions from multiple radios [1]. The advantage is based on array gain (increased collective average transmit power compared to a single transmitter) and diversity gain, assuming uncorrelated fading channel conditions. When this SNR advantage is used to extend the communication range, the performance of network layer can be enhanced in terms of network connectivity [2], broadcasting and unicasting in fewer hops [3], [4], and energy balancing [5]. Very few demonstrations of concurrent (i.e., simultaneous transmission) CT with practical synchronization have been reported [6]. This paper is the first report of a systematic study of a CT range extension in an indoor environment, where experimental results are compared with a theoretical model.

CT methods may be classified into three categories, according to their synchronization requirements at the transmitters: coherent beamforming, concurrent CT (CCT), and time-division CT (TDCT). Coherent beamforming requires feedback of channel state information to the transmitters, so the phases of their transmissions will align at the receiver [7]; this phase synchronization requires significant network overhead. CCT requires that each transmitter choose or be allocated a diversity channel (i.e., an orthogonal dimension) in which to transmit, from a set of at least two orthogonal channels (different linear combinations of diversity channels can also be allocated [8]). Ideally, each receiver gets approximately equal average power in each diversity channel, to achieve the maximum diversity order. However, disparities in average power, from unequal path loss or poor allocation, can diminish the effective diversity order of CCT. The synchronization requirements of CCT are that the transmissions need to arrive at the receiver with sufficiently small relative time offsets and relative carrier frequency offsets, so that the signal can be processed as though it came from a single transmitter through a multipath channel with reasonable delay and Doppler spreads. In TDCT, a receiver synchronizes to only one time offset and carrier frequency offset at a time. However, in a range extension scenario, each copy it receives could be very weak, leading to poor start-of-packet estimation for each copy. To achieve the SNR advantage, the copies must be well aligned, at least in time, leading to potentially high complexity in the receiver. Of the three categories, CCT has particular advantages for range extension, because the receiver can exploit the SNR advantage in synchronization without high complexity [9].

II. Experimental Setup

A. Experimental Design

The purpose of this study is to compare the maximum range reached in two hops by conventional non-CT and CCT. For the conventional non-CT, the two hops are built with two consecutive single-input-single-output (SISO) links. For CCT, as shown in Fig. 1, the first-hop links are also SISO links as in non-CT. However, the second-hop link is multiple input and single output (MISO), created by multiple physically separate radios and a single destination radio, so that CCT synchronization can exploit diversity. We measure the average packet error rate (APER) at the second-hop receiver (destination), where the average is taken over 120 multipath fading channel realizations.

The 120 channel realizations are achieved as follows. First, as shown in Fig. 2(a), we placed 15 radios on the receiver cart with a sufficient inter-element spacing ($\sim$1.5 wavelengths), which satisfies the conditions for the uncorrelated multipath fading and suppresses the mutual coupling effect [10]. The 15 radios on the receiver side are just for the purpose of creating 15 multipath channels at the same time in one measurement phase of 1,000 packets. Second, we moved each of the four

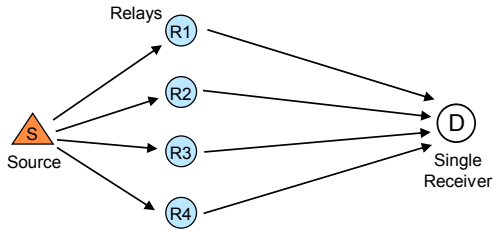

Fig. 1. The logical topology for the experiment

(a) Receiver cluster (b) A relay node

Fig. 2. Equipment setting

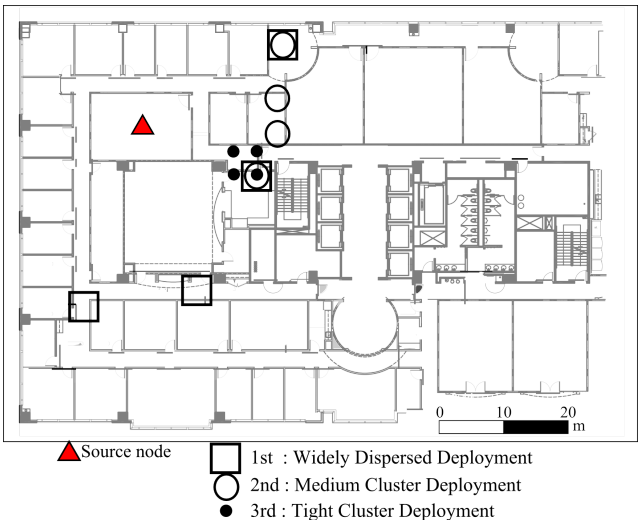

Fig. 3. The floor plan and the three measurement campaigns

relays (see one relay in Fig. 2(b)) around to eight distinct locations in a local area. Through this procedure, we can achieve $15 \times 8 = 120$ channel realizations. For the comparison between the conventional non-CT (SISO) and CCT, we have chosen the best (lowest) APER among the four SISO APERs, and compared it with the CCT APER.

B. Measurement Campaign

The measurements were conducted on the fifth floor of the Centergy building of the Georgia Institute of Technology, Atlanta, GA. Fig. 3 shows the floor plan of this typical academic office building consisting of research laboratories, offices and conference rooms. There are several straight corridors with offices on the one side and relatively large laboratories on the other. The interior walls of the building are made of wallboard with steel studs, and the stairwells and the elevator columns are made of reinforced concrete. For this reason, the center of the building around the elevator lobby attenuates radio signals significantly.

The measurement campaign consists of three stages corresponding respectively to the three relay topologies displayed in Fig. 3. The three topologies are $i)$ widely dispersed (indicated by the squares), $ii)$ medium cluster deployment (the circles), and $iii)$ tight cluster (the dots). For all three topologies, the relays are maximally far from the source such that the first-hop APER is less than 0.01, so that we can focus more on the second-hop decoding range. The second-hop decoding region is defined as the area where the second-hop APERs are less than or equal to 0.1. Of course, the decoding region will change depending on the receiver sensitivity and the transmit power. Any changes in the ratio of transmit power to receiver sensitivity that are large enough to change the shadowing statistics would change the relative sizes of CT and non-CT decoding regions.

The three topologies were motivated by the following considerations. Wireless channels exhibit path loss, multipath fading, and shadowing. If the relays are close enough to share the same path loss and shadowing, yet have sufficient separations (at least a half wavelength in an indoor environment) to achieve uncorrelated multipath fading in their channels, then CT can deliver the maximum micro-diversity gain; this is what a real array antenna (i.e., when the transmitters are connected by wire on the same platform) typically delivers. However, with CT, the elements in the *virtual array* are less constrained, because they are actually separate radios not connected by wire. Therefore, if the CT radios are separated by more than the shadowing correlation distance (e.g., about 1.7 meters for indoor NLOS channel [11]), then macro-diversity gain is also achievable. However, the path losses would be very different if the inter-element spacing is very large, which would be the case in a low-density network; then some relays' contributions to the diversity gain will be very small, possibly leading to an effective diversity order less than the number of relays doing CT. Therefore, our aim in designing the cluster topologies was to capture the three cases of: micro diversity only (tight), full-order micro and macro diversity (medium), and reduced effective diversity (widely dispersed) because of disparate path losses.

C. Node Description

Each wireless node was implemented by an Ettus RF daughterboard, a Universal Software Radio Peripheral 1 (USRP1) [12], and GNU radio [13] on a personal computer (PC). The transmit frequency of the source (the receive frequency of the first-hop receivers) was 2.482GHz. In the second-hop, each transmitter used a unique carrier frequency, with 128 kHz separation between adjacent carrier frequencies, to create the orthogonal diversity channels. The collection of carriers was centered at 2.492GHz to avoid WiFi interference. Non-coherent BFSK was chosen for its good energy efficiency

and low implementation complexity. Also, no error-correction coding was used. Equal gain combining and a mean-based method of transmit time synchronization was used [9]. In order to minimize the distortion caused by the different hardware, we calibrated the receiver sensitivity of all the radios. The packet in this experiment was 22 bytes long which consists of 4 bytes preamble, 6 bytes header, 10 bytes data and 2 bytes CRC. A relay node decides to transmit only if CRC check passes.

D. Log-distance Path Loss Model

In this section, we explain how we extract from our SISO PER measurements a channel model for our building, which includes the path loss exponent and lognormal shadowing parameter. In the next section, we use these parameters to calculate APER outage rate and compare the measured data to a theoretical model.

First, without considering burst errors, the relationship between PER and BER for the ith multipath realization can be formulated by

$$BER_i = 1 - (1 - PER_i)^{1/D}, \tag{1}$$

where D is the packet length in bits which is 176 in our experiment. For non-coherent BFSK modulation, the bit error rate as a function of the received SNR γ_i is

$$BER_i = \frac{1}{2}\exp(-\frac{1}{2}\gamma_i), \tag{2}$$

where $\gamma_i = \alpha_i^2 E_b/N_0$, where E_b is the bit energy, N_0 is the noise power spectral density, and α_i is the channel gain of the ith multipath realization (assumed constant during the 1,000 packets used to calculate PER_i). Thus, by combining (1) and (2), we can get an unique value of γ_i for each unique value of PER_i that we measure. Next, we can calculate the average received SNR, averaged over 120 channel realizations within the local area of the receive location, as

$$\overline{\gamma} = \frac{1}{120}\sum_{i=1}^{120}\gamma_i. \tag{3}$$

Now, we can apply the log-distance path loss model to our second-hop. Let d be the distance from the transmitter (relay) to the destination (the second-hop receiver), d_0 be the reference distance, and n be the path loss exponent, where d_0 is a short reference distance that is in the far field of the antennas but short enough that free-space path loss applies, and X_σ is a random variable representing shadowing (Gaussian distribution in dB scale with zero-mean and standard deviation σ), then the received power $P_R(d)$ is given by

$$P_R(d)_{(\text{dBm})} = 10\log_{10}\frac{P_R(d_0)}{0.001W}{}_{(\text{dBm})} - n\log_{10}\frac{d}{d_0}{}_{(\text{dB})} + X_{\sigma(\text{dB})}. \tag{4}$$

Since the radios are all calibrated to have the same noise power spectral density, the log-distance path loss model can be rewritten in terms of average SNR in the dB scale as

$$\overline{\gamma}(d)_{(\text{dB})} = \gamma(d_0)_{(\text{dB})} - n\log_{10}\frac{d}{d_0} + X_{\sigma(\text{dB})}. \tag{5}$$

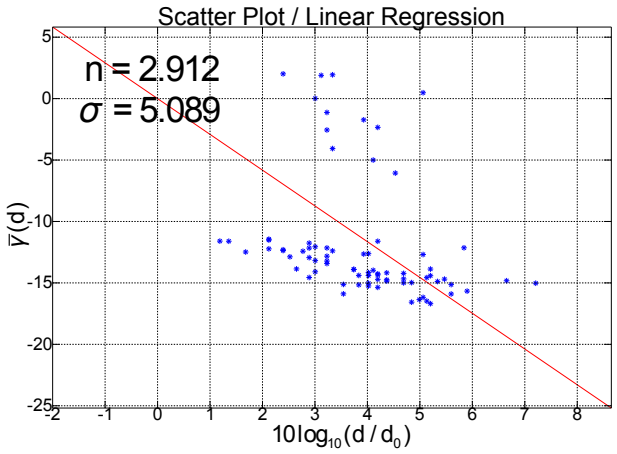

Fig. 4. Scatter plot of $\overline{\gamma}(d)$ and its linear regression

The standard procedure for estimating n and σ is to do a linear regression on the set of ordered pairs $(d, \overline{\gamma}(d))$, with the constraint that the line passes through $(d_0, \gamma(d_0))$ [14]. Fig. 4 displays all measured path loss values versus log-distance derived from (5). As shown in Fig. 4, the linear regression gave the path loss exponent of n=2.912 and the standard deviation of shadowing of σ=5.089 which are similar to the numbers reported for 2.5GHz and indoor environments in [15] (e.g., n=2.4, σ=5.8). The dots above the red straight line correspond to the relatively low path losses in corridors or the paths not undergoing the significant attenuation by the elevator lobby. In contrast, the scatters below the line are from the measurement locations having the SISO paths with relatively large attenuation of multiple walls or the elevator lobby, which results in lower SNRs.

E. CCT Outage Rate Model

We consider APER>0.1 to be an outage. Using (1) and (2) this APER threshold of 0.1 can be trasnsformed into an SNR threshold of about 11.3dB. Using the values of n and σ from the previous section, we can define the outage probability for a SISO link as

$$\Pr\{\overline{\gamma}(d)_{(\text{dB})} < 11.3\text{dB}\} = 1 - Q(\frac{11.3 - \mu_{\overline{\gamma}}(d)}{\sigma}), \tag{6}$$

where $\mu_{\overline{\gamma}}(d)$ is the expected value of $\overline{\gamma}(d)$ in (5) over the different shadowing effects X_σ. For example, $\Pr\{\overline{\gamma}(d)_{(\text{dB})} < 11.3\text{dB}\} = 0.02$ would mean that there is a 2% chance that APER>0.1.

However, when it comes to CCT, obtaining a closed form for outage probability is difficult because of the multiple transmitter-receiver pairs with correlated shadowing. The diversity combining scheme in the experiment is non-coherent (post-detection) equal gain combining where the total received SNR is the sum of SNR from each link [16]. Hence, when the number of transmitter is L, the outage probability is given by

$$\Pr\{\gamma_{cct} < 10^{11.3/10}\} = \Pr\{\sum_{k=1}^{L}\gamma(d_k) < 10^{11.3/10}\}, \tag{7}$$

where d_k is the distance from the kth first-hop relay to the destination at the second-hop. When k is the index for the each link, and i is the index for one multipath trial, the random variable $\gamma(d)$ is determined by path loss, multipath fading, and shadowing as $\gamma_i(d_k) = \alpha_i^2(d_k) \cdot (E_b/N_o) \cdot X_{\sigma(k)}$. With Rayleigh fading, $\alpha^2(d_k)$ follows the exponential distribution. Also, $X_{\sigma(k)}$ is spatially correlated shadowing for different paths indexed by k. We can apply the correlation model in [17] to our situation where multiple transmitters have the receivers at the same location which gives the correlation of the two links with the transmitter separation of d_S as

$$R(s) = \sigma^2 e^{-d_S/D_S}, \tag{8}$$

where D_S is the decorrelation distance, which means the distance from one transmitter to another such that the correlation is dropped by a factor of e^{-1}. [11] presented the decorrelation distance of $1.7m$ measured from similar indoor environments with the center frequency of 1.8GHz.

III. Experimental Results

The experimental second-hop decoding regions and the APERs of the three relay deployments are depicted in Fig. 5(a), 6(a), and 7(a). The red triangles represent the source node, and the blue circles are the relays. The SISO decoding region is indicated by the light-gray areas, and the CCT decoding range is the union of the light-gray and dark-gray areas. The green squares are labeled with the APERs of some selected SISO destinations on the SISO decoding range boundaries. The white-filled circles indexed by the letters from A to V are labeled by APERs for 4-relay CCT. As stated in the previous section, the APERs on the green squares and white-filled circles were averaged over 120 multipath path realizations. However, the APERs to decide the light and dark gray areas are averaged over only 15 multipath trials, and the measurements were made at approximately $3m$ intervals. The CCT destination locations are not the same for each topology, but there are some common locations. For example, A, B, C and D are common for all. Also, E and F are common to the widely dispersed and medium cluster deployments. Lastly, 7 measurement locations (L, M, N, O, P, Q, and R) are shared by the medium cluster and tight cluster deployments.

We consider two evaluation criteria: directional range extension and coverage area extension. Directional range extension is the increase of the second-hop decoding range from non-CT to CCT in one direction. Directional range extension is important, for example, in overcoming the energy hole problem [5]. Coverage area is one of the most popular network design factors. Maximizing coverage area often corresponds to minimizing cost.

We note that the two evaluation quantities are strongly influenced by the location of the source within the building. In our experiments, the source was near to the upper left corner of the building, and the relays were placed to the opposite side of the corner instead of surrounding the source. Therefore, the coverage areas are not discs but sectors. For this reason, we did not measure APERs on the left upper side of the building around the source (the white region surrounded by the light-gray area in the figures). Also, the heavy attenuation of the elevator lobby (the seven squares around H in Fig. 5(a)) and the bathrooms (on the right of the elevator lobby) limit the range extension in that direction. If the measurements were performed in a part of the building away from the building core, we expect that the range and coverage extension values would be higher.

A. Directional Range Extension

The "direction" of the one-dimensional range extension in our experiment can be defined as the direction in which the second-hop decoding range is maximized. Let $\mathcal{S}_c$ be the set of locations (x_c, y_c) on the outer border of the CCT coverage region. Suppose (x_k, y_k) is the location of the kth relay, then we can define the direction based on

$$(x_c', y_c') = \arg \max_{(x_c, y_c)} [\min_k |(x_c, y_c) - (x_k, y_k)|]. \tag{9}$$

This means (x_c', y_c') is the point that maximizes the distance from the closest relay and itself. However, this definition does not consider the SISO range. For example, in the widely dispersed and the medium cluster cases, the directions would be toward the upper right edge of the dark-gray area around E in Fig. 5(a) and 6(a) which is a LOS channel path where the SISO range is also long. Therefore, we introduced another definition for the direction as

$$(x_c', y_c') = \arg \max_{(x_c, y_c)} [\min_k \left| \frac{(x_c, y_c) - (x_k, y_k)}{(x_s, y_s) - (x_k, y_k)} \right|], \tag{10}$$

where $(x_s, y_s) \in \mathcal{S}_s$ is the longest-range SISO reception point located on the straight line between (x_c, y_c) and its closest relay. The resulting directions of the topologies are indicated by the yellow stars in Fig. 5(a), 6(a), and 7(a). The ratios $\rho_d = |[(x_c, y_c) - (x_k, y_k)]/[(x_s, y_s) - (x_k, y_k)]|$ in (10) are given in the "experiment" column of Table I. The reason why the widely dispersed topology had the lowest ρ_d is because some relays are far from the destination, and hardly contribute to the improvement in APERs because of their significant path losses. On the contrary, the medium cluster exploits both micro and macro diversity, which gives the large ρ_d. On the other hand, the range extension of the tight cluster is based only on the array gain and micro diversity.

B. Coverage Area

We define the second-hop coverage area to include all destination locations within the decoding range of the four relays. We define the fraction

$$\rho_c = \frac{\text{second-hop CT decoding area}}{\text{second-hop SISO decoding area}}. \tag{11}$$

The denominator is the light-gray area and the numerator is the union of the light-gray and dark-gray areas. The results shown in the "experiment" column in Table II seem to favor the tight cluster topology, but they hide the fact that the total CCT second-hop coverage area for the widely dispersed topology is larger than that of the other two. Also, the experimental results

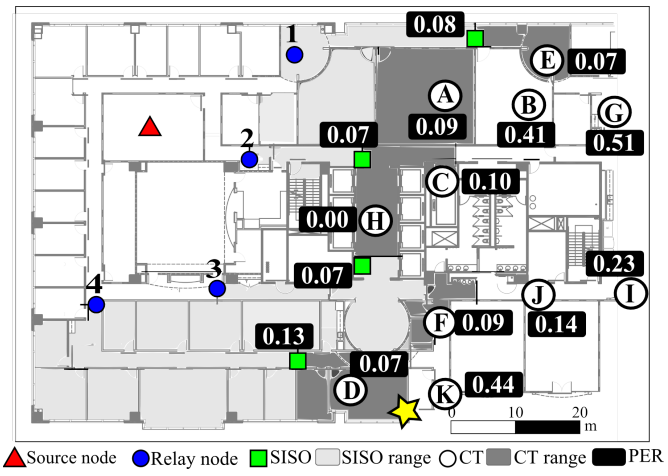

(a) the measured range extension and APERs

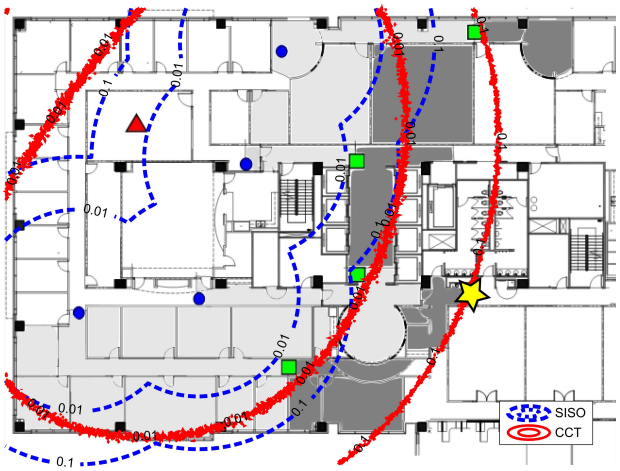

(b) the contour lines from simulation

Fig. 5. Topology I : Widely dispersed deployment

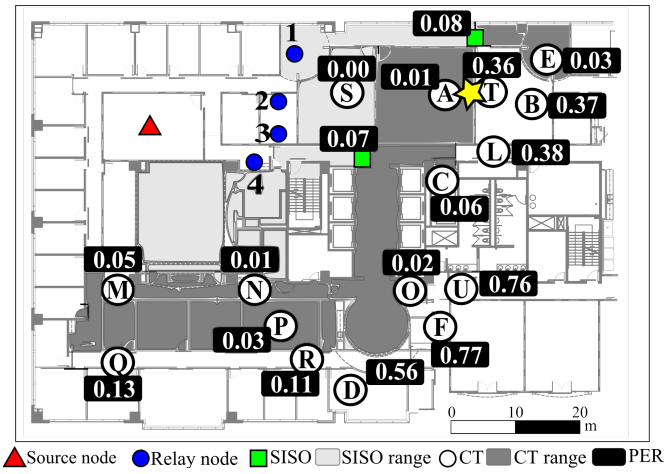

(a) the measured range extension and APERs

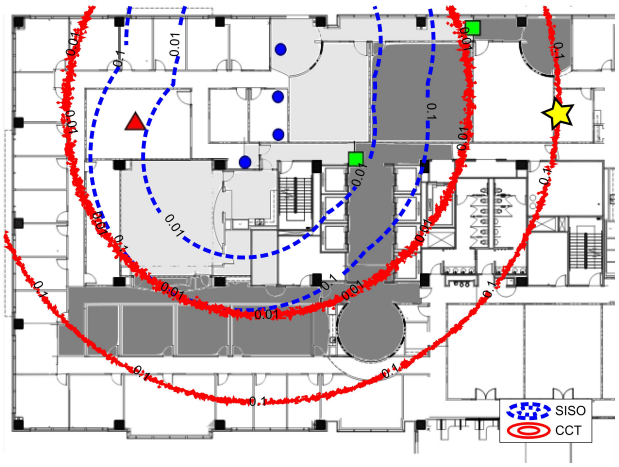

(b) the contour lines from simulation

Fig. 6. Topology II : Medium cluster deployment

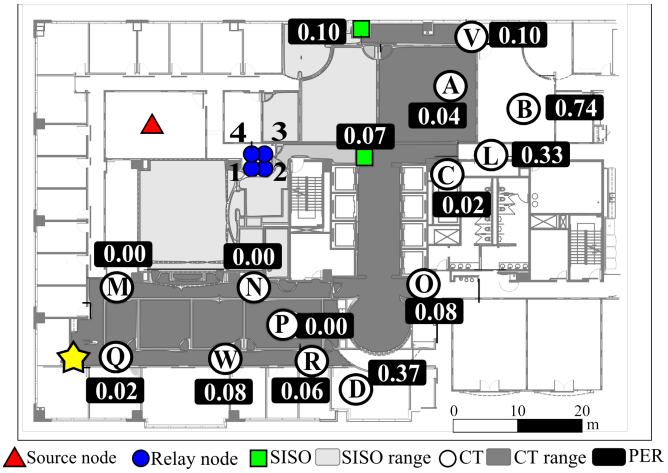

(a) the measured range extension and APERs

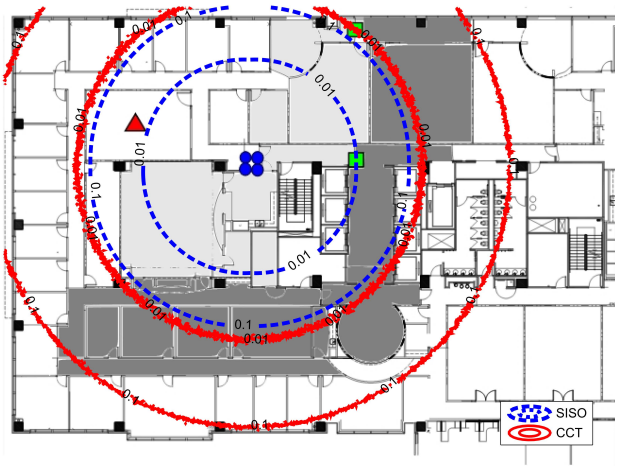

(b) the contour lines from simulation

Fig. 7. Topology III : Tight cluster deployment

would vary, if the source location were not in the corner of the building. Another consideration is that the widely dispersed topology showed larger SISO coverage since it had much longer relay inter-spacing and allowed the placement of relay nodes in corridors, so favorable LOS propagation condition is given.

C. Comparison with the Simulation Results

The results of the simulation are provided in Fig. 5(b), 6(b), and 7(b). The two blue dashed-contour lines represent the SISO destination locations with the outage probability of 0.01 (inner) and 0.1 (outer). Likewise, the two red solid lines correspond to the CCT destination locations with the outage probability of 0.01 (inner) and 0.1 (outer). We remind the reader that these numbers are not APERs, rather, they are the probabilities that the random APERs (because of shadowing) are greater than 0.1. The light-gray and dark-gray regions are copied from Fig. 5(a), 6(a), and 7(a), respectively, for reference.

One way to think about an outage rate contour is the following. If one imagines walking along a contour, for example, the 1% outage rate contour, then if the model is correct, one should find oneself in outage (i.e., outside of the relevant gray area) about 1% of the time. Therefore, the SISO 1% contour, for example, should be almost entirely inside the light gray area. With this interpretation in mind, we observe that the 1% contours for each of SISO and CT appear to fit the data well. On the other hand, the 10% contour appears to be too far away from the relays. For example, in both the medium and tight relay topologies, the 10% contour is almost entirely outside of the gray areas.

This discrepancy could be due to inaccuracy in our parameter estimates, either because of the small sample or because we ignored burst bit errors. If could also be attributed to the simplicity of the log-distance path model ("multi-slope" models may be more appropriate [14]). Regarding directional range extension, we observe from the measured data in Fig. 5(a), 6(a), and 7(a) that the location of the yellow star is approximately broadside to the virtual array of relays (by "broadside", we mean along a line that is nearly a perpendicular bisector of the "line" of the array).

The outage rate contours for the widely dispersed and medium relay topologies produce yellow star locations that are also approximately broadside to the array. However, there can be no such correspondence between measurement and theory in the tight cluster case, because the contours are circles.

IV. Conclusion

This paper presents experimental directional coverage extension by CCT in terms of average PERs in a typical modern office environment. Three relay topologies are distinguished by the presence or absence of the features: disparate path loss to the destination, micro diversity, and macro diversity. It has been shown that the widely dispersed topology is effective to maximize the coverage area while the medium cluster is best for the directional range extension. The measured data matched well the 1% outage contour, but had a poor match to the 10% outage contour. The overall conclusion is that CCT is an effective and practical way to extend range and coverage area in an indoor environment.

TABLE I
ρ_d AND THE DIRECTIONS OF THE EXPERIMENT AND THE SIMULATION

topology	experiment	0.1 contour	the direction difference
Widely dispersed	1.93	1.66	different (31.1°)
Medium cluster	2.18	1.84	almost same (5.7°)
Tight cluster	2.10	1.62	simulation: omnidirectional

TABLE II
ρ_c OF THE EXPERIMENT AND THE SIMULATION

topology	experiment	0.01 contour	0.1 contour
Widely dispersed	1.589	1.634	1.568
Medium	2.546	2.361	2.394
Tight cluster	2.700	2.533	2.357

References

[1] J. Laneman, D. Tse, and G. Wornell, "Cooperative diversity in wireless networks: Efficient protocols and outage behavior," *IEEE Trans. on Information Theory*, vol. 50, no. 12, pp. 3062–3080, Dec. 2004.

[2] A. Scaglione and Y.-W. Hong, "Opportunistic large arrays: cooperative transmission in wireless multihop ad hoc networks to reach far distances," *IEEE Trans. on Signal Processing*, vol. 51, no. 8, pp. 2082–2092, Aug. 2003.

[3] B. Sirkeci-Mergen, A. Scaglione, and G. Mergen, "Asymptotic analysis of multistage cooperative broadcast in wireless networks," *IEEE Trans. on Information Theory*, vol. 52, no. 6, pp. 2531 – 2550, June 2006.

[4] L. Thanayankizil, A. Kailas, and M. A. Ingram, "Routing for wireless sensor networks with an opportunistic large array (OLA) physical layer," *Ad Hoc & Sensor Wireless Networks*, vol. 8, no. 1-2, pp. 79–117, 2009.

[5] J. W. Jung and M. A. Ingram, "Residual-energy activated cooperative transmission (REACT) to avoid the energy hole," *IEEE ICC Workshop on CoCoNet3*, June 2010.

[6] A. Blair, T. Brown, K. M. Chugg, and M. Johnson, "Tactical mobile mesh network system design," *IEEE MILCOM*, pp. 1 –7, Oct. 2007.

[7] R. Mudumbai, D. Brown, U. Madhow, and H. Poor, "Distributed transmit beamforming: challenges and recent progress," *IEEE Comm. Mag.*, vol. 47, no. 2, pp. 102–110, Feb. 2009.

[8] B. Mergen and A. Scaglione, "Randomized space-time coding for distributed cooperative communication," *IEEE ICC on Comm.*, vol. 10, pp. 4501 –4506, June 2006.

[9] Y. J. Chang, M. A. Ingram, and S. Frazier, "Cluster transmission time synchronization for cooperative transmission using software defined radio," *IEEE ICC Workshop on CoCoNet3*, June 2010.

[10] P.-S. Kildal and K. Rosengren, "Correlation and capacity of MIMO systems and mutual coupling, radiation efficiency, and diversity gain of their antennas: simulations and measurements in a reverberation chamber," *IEEE Comm. Mag.*, vol. 42, no. 12, pp. 104 – 112, Dec. 2004.

[11] N. Jalden, P. Zetterberg, B. Ottersten, A. Hong, and R. Thoma, "Correlation properties of large scale fading based on indoor measurements," *IEEE WCNC*, pp. 1894 –1899, Mar. 2007.

[12] "Universal sofrware radio peripheral," http://www.ettus.com.

[13] "Gnu radio," http://gnuradio.org.

[14] T. Rappaport, *Wireless Communications: Principles and Practice*. Upper Saddle River, NJ, USA: Prentice Hall PTR, 2001.

[15] C. Anderson and T. Rappaport, "In-building wideband partition loss measurements at 2.5 and 60 ghz," *IEEE Trans. on Wireless Comm.*, vol. 3, no. 3, pp. 922 – 928, May 2004.

[16] M. K. Simon and M.-S. Alouini, *Digital Communication over Fading Channels*. Wiley-IEEE Press, 2002.

[17] M. Gudmundson, "Correlation model for shadow fading in mobile radio systems," *Electronics Letters*, vol. 27, no. 23, pp. 2145 –2146, 7 1991.